Photonic Crystal Lasers



Room-Temperature InGaAs Nanowire Array Band-Edge Lasers on Patterned Silicon-on-Insulator Platforms

Hyunseok Kim,* Wook-Jae Lee, Ting-Yuan Chang, and Diana L. Huffaker

Integration of ultracompact light sources on silicon platforms is regarded as a crucial requirement for various nanophotonic applications. In this work, InGaAs/InP core/shell nanowire array photonic crystal lasers are demonstrated on silicon-on-insulator substrates by selective-area epitaxy. 9×9 square-lattice nanowires forming photonic crystal cavities with a footprint of only $3.0\times3.0\,\mu\text{m}^2$, and a high Q factor of 23 000 are achieved by forming these nanowires on two-dimensional silicon gratings. Room-temperature lasing is observed from a fundamental band-edge mode at 1290 nm, which is the O-band of the telecommunication wavelength. Optimized growth templates and effective in-situ passivation of InGaAs nanowires enable the nanowire array to lase at a low threshold of 200 μ J cm $^{-2}$, without any signature of heating or degradation above the threshold. These results represent a meaningful step toward ultracompact and monolithic III–V lasers on silicon photonic platforms.

Integration of compact lasers on silicon platforms has been of keen interest in photonic communities for over a decade, which could be utilized for chip-scale optical interconnects, photonic integrated circuits, optical computing, and photonic sensing platforms. [1–3] III–V semiconductors with direct bandgaps are typically employed as gain media in these lasers due to the indirect nature of silicon's electronic band structure. Bonding methods such as flip-chip bonding and wafer bonding are the most widely used techniques to integrate III–V lasers on silicon, although the requirement of III–V wafers makes this process

Dr. H. Kim, T.-Y. Chang, Prof. D. L. Huffaker Department of Electrical and Computer Engineering University of California Los Angeles Los Angeles, CA 90095, United States E-mail: hyunseokkim@ucla.edu

Dr. W.-J. Lee School of Engineering Cardiff University Cardiff CF24 3AA, United Kingdom

Dr. W.-J. Lee Electronics and Telecommunications Research Institute Daejeon 34129, South Korea

Prof. D. L. Huffaker School of Physics and Astronomy Cardiff University Cardiff CF24 3AA, United Kingdom Prof. D. L. Huffaker California Nano-Systems Institute University of California Los Angeles Los Angeles CA 90095, United States

DOI: 10.1002/pssr.201800489

costly.^[4,5] As an alternative approach, direct growth of III–V materials on silicon has also been extensively studied to eliminate bonding processes. However, epitaxially integrated materials are highly defective because of the lattice mismatch, and even with the introduction of thick metamorphic buffer layers, the material quality is still inferior to III–V epilayers grown on III–V substrates.^[6,7]

Besides III–V compound semiconductors, solution-processed perovskites are regarded as one of the promising materials for on-chip lasers due to their superior optical properties,^[8] and monolithic integration of perovskite lasers on silicon photonic chips^[9] and perovskite nanowire-based lasers^[10] are recently reported. Two-dimensional van der Waals materials are also explored as a candidate for on-chip lasers.^[11] Although these emerging materi-

als have huge potential for functional and efficient lasers, the bandgap of these materials are typically large and it is challenging to achieve lasing around telecom wavelengths for silicon photonic applications.

Epitaxy of III-V nanowires has been recently proposed as a new technique to monolithically integrate high-quality III-V materials on silicon platforms. Extremely small interface area between nanowires and silicon allows effective relaxation of strain in nanowires and therefore high-quality nanowires can be grown despite the large lattice mismatch. [12,13] Furthermore. nanowires with smooth sidewalls naturally support propagating modes in the nanowires, and Fabry-Perot cavities can be formed from single nanowire by exploiting its waveguiding properties and end-facet reflection. [14,15] Nanowire approach therefore provides a way to directly construct ultracompact lasers on silicon. However, optical confinement in free-standing nanowires on silicon is typically weak due to the low reflectivity between the interface of nanowire and silicon, and this increases the threshold gain of nanowire lasers, resulting in vertical nanowire lasers on silicon to operate in a cryogenic environment.[16-19]

To circumvent this limitation and achieve room-temperature operation, we have recently proposed that optical confinement can be significantly improved by forming photonic crystal cavities based on two-dimensional (2D) nanowire arrays.^[20] These nanowires are integrated on silicon grating structures of 220 nm-thick silicon-on-insulator (SOI) substrates, which is a standard SOI thickness in photonic industries,^[21] and provides additional functionalities such as vertical confinement and

www.pss-rapid.com

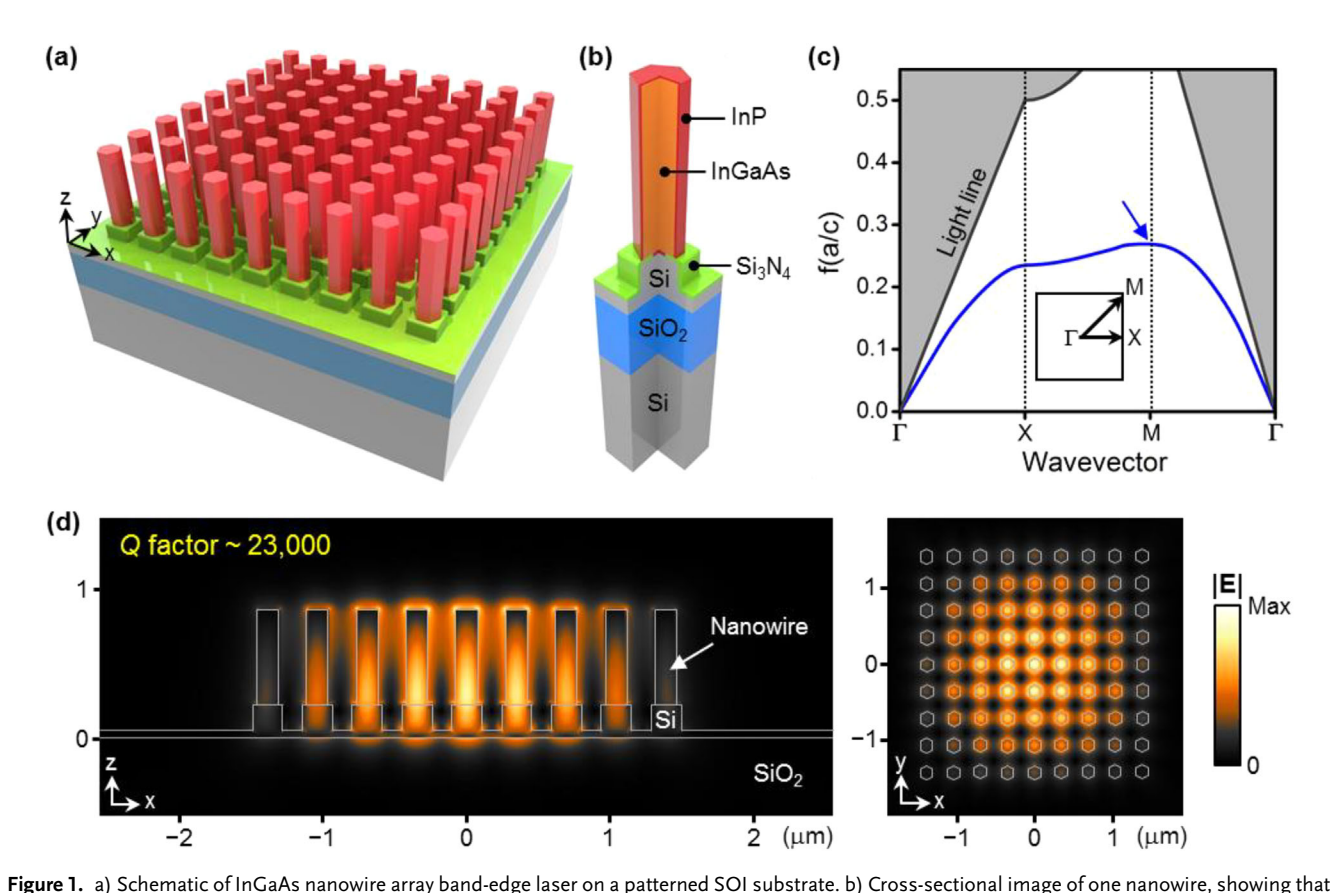
waveguide coupling. Although lasing has been achieved from 2D nanowire arrays on planar SOI substrates^[22] and 1D nanowire arrays, ^[23,24] experimental demonstration of 2D nanowire arrays on gratings is still yet to be achieved.

Here, we demonstrate room-temperature lasing from 2D nanowire arrays on patterned SOI platforms. InGaAs/InP core/shell nanowires are grown on silicon 2D gratings by selective-area epitaxy, which enables the formation of high-Q cavities on SOI. The nanowire laser operates at a fundamental photonic band-edge mode near 1300 nm, a technologically important wavelength for silicon photonics.

A schematic illustration of proposed nanowire array lasers is depicted in **Figure 1a**. An SOI substrate with a silicon layer thickness of 220 nm and a buried oxide layer thickness of 2 μ m is employed, wherein 2D silicon gratings are formed by etching the silicon layer by 180 nm. Eighty-one nanowires are integrated on gratings to form a 9 \times 9 square-lattice, and 20 nm-thick silicon nitride (Si₃N₄) layer is employed as a nanowire growth mask. Each nanowire is composed of InGaAs core region as an active medium and InP shell for surface passivation, as shown in the cross-sectional image of a single nanowire in Figure 1b, where shells with a low surface recombination velocity and a large bandgap improve quantum efficiency of nanowires.^[25]

Photonic band structure for an infinite array of nanowires is calculated using 3D finite-difference time-domain (FDTD)

method, assuming that the refractive index of InGaAs is 3.62. [26] The diameter (*d*) and height (*h*) of nanowires used in the simulations are 176 and 680 nm, respectively, which are actual dimensions of as-grown nanowires. Rectangular silicon gratings with a width of 180 nm is encapsulated by 20 nm-thick silicon nitride, and the lattice constant (a) is 350 nm. Figure 1c shows the calculated band structure of the fundamental TM mode plotted with the light line of air. We employ the M-point bandedge mode (blue arrow) as a lasing mode, because this mode exhibits the highest cavity Q factor. In reality, the lattice size is finite and the Q factor increases with the lattice size. [27,28] When the array size is 9×9 , which is the case of our design, the Q factor of the M-point band-edge mode was calculated to be 23 000, which is more than an order of magnitude higher than single nanowire-based Fabry-Perot laser cavities, [16,17] and the resonant wavelength was 1286 nm. On the other hand, if such 9×9 nanowire array is on 220 nm-thick SOI without gratings, then confined mode is not observed due to substantial leakage of electric fields through silicon. Therefore, forming trenches around each nanowire is critically important to achieve a high cavity Q factor. The calculated electric field profile of the M-point band-edge mode is shown in Figure 1d. Vertical and horizontal cross-sectional profiles show that the field is tightly confined in nanowires, and the confinement factor, Γ , is calculated to be 0.52, where such a high confinement factor is beneficial for



InGaAs nanowire array band-edge laser on a patterned SOI substrate. b) Cross-sectional image of one nanowire, snowing that InGaAs nanowires are passivated by InP shells and each nanowire is integrated on a silicon grating structure. c) In-plane photonic band structure of nanowire array cavity. d) Electric field profiles of the fundamental TM mode (blue arrow in (c)). (left) Vertical cross-section of the center row, and (right) horizontal cross-section the nanowire array. Si₃N₄ layer is not drawn in the images for visibility, but is included in simulations.

the edge effect by blocking the diffusion of adatoms, so that nanowires in the center and the edge of the array have uniform dimensions to form high-Q cavities.

Nanowires are grown on the prepared SOI platform using a metal-organic chemical vapor deposition (MOCVD) system. Trimethylindium (TMIn), Triethylgallium (TEGa), tertbutylarsine (TBAs), and tert-butylphosphine (TBP) are used as precursors. The sample is first baked at 850 °C in the MOCVD reactor to thermally etch native oxide. Next, InGaAs nanowires are grown at 655 °C under a gas-phase indium composition (TMIn/(TMIn+TEGa)) of 45%, followed by InP shell growth at 600 °C. Detailed growth conditions can be found in Experimental Section. As shown in the SEM images in Figure 2b, vertical InGaAs/InP core/shell nanowires are integrated on 2D silicon gratings. Nanowires exhibit uniform diameter and height without any distinguishable edge effect, while non-uniform polycrystalline structures are grown on the mask opening area surrounding the trench because the growth conditions such as V/III ratio and temperature are optimized for nanowires, not for thin films.

The nanowire array cavity is characterized at room temperature by optically pumping the array using a 660 nm wavelength pulsed laser with a pulse width of 30 ps. The emission from nanowires is resolved using a spectroscopy equipped with a commercial InGaAs detector (detailed measurement setup in Experimental Section). At a low pump power, a broad spontaneous emission peak is observed as shown in the log-scale photoluminescence (PL) spectra in **Figure 3**a, and the solid phase indium composition in InGaAs nanowires is deduced to be around 40% from the spectra. As the pump power is increased, a stimulated emission peak around 1290 nm appears,

low-threshold lasing since threshold power is inversely proportional to Γ . It is also worth mentioning that the electric field intensity gradually decreases from the center to the edge of the lattice, which is in contrast to photonic crystal cavities with artificial defects wherein the field is tightly confined only in the defect area. ^[29] This makes band-edge lasers more suitable for the applications requiring higher output power. ^[30] It should also be noted that the proposed bottom-up nanowire array cavity has extremely small footprint, with the size of only $3.0 \times 3.0 \,\mu\text{m}^2$.

An SOI(111) wafer with a silicon layer thickness of 2 µm and a buried oxide layer thickness of 2 µm is used for the fabrication of band-edge lasers. The silicon layer is first thinned to 220 nm by thermal oxidation and oxide removal processes, and then 180 nm-deep trenches are formed on the silicon layer by e-beam lithography and dry etching. Next, a 20 nm-thick silicon nitride (Si₃N₄) layer is conformally deposited, followed by e-beam lithography to expose silicon for selective-area nanowire epitaxy. Detailed fabrication processes can be found elsewhere. [31] SOI patterns prepared for the nanowire growth are shown in the scanning-electron microscope (SEM) images in Figure 2a. Alignment markers are employed to precisely position nanoholes at the center of each grating (inset in the lower SEM image of Figure 2a). A 1.2 µm-wide trench is formed around the 2D gratings to isolate the cavity, and 4 µm-wide opening of silicon nitride mask is made outside the trench to expose silicon for uniform nanowire growth. When nanowires are grown by selective-area epitaxy method, the nanowires at the edge of an array are typically taller or fatter than the center nanowires. [32-34] This is due to additional supply of materials to edge nanowires by diffusion of adatoms from external mask area, which is known as an edge effect. The role of mask openings here is to minimize

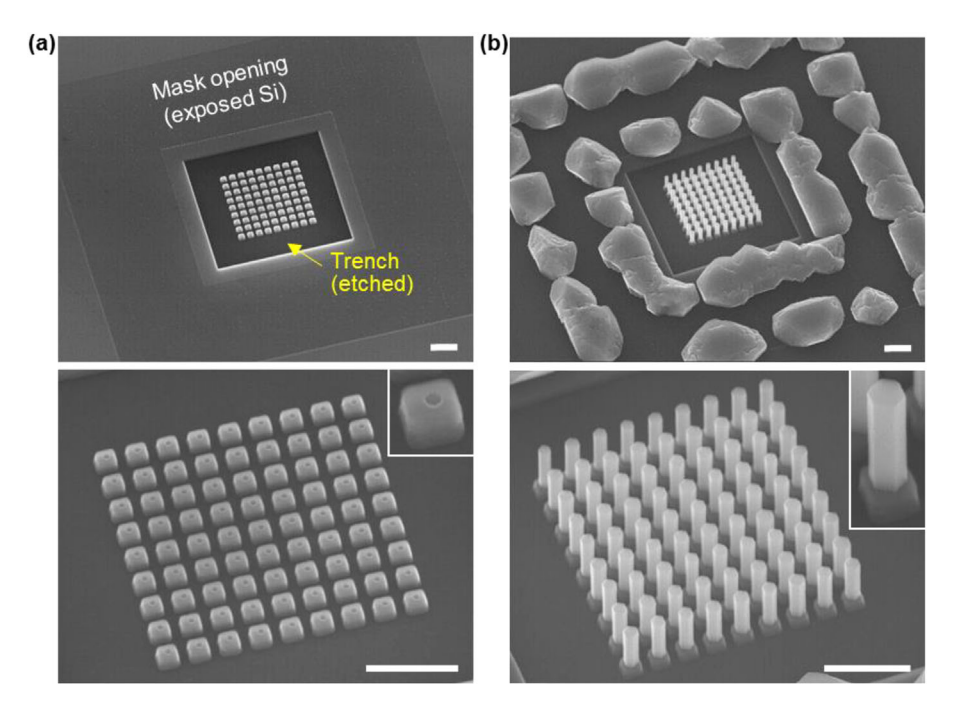


Figure 2. SEM images of SOI platforms (a) prepared for nanowire growth, and (b) after the nanowire growth. The upper images are overall views of entire structures, and the lower images are close-up views of the cavity area. Insets in the lower images show one of the gratings before and after the growth. Scale bars: 1 μm.

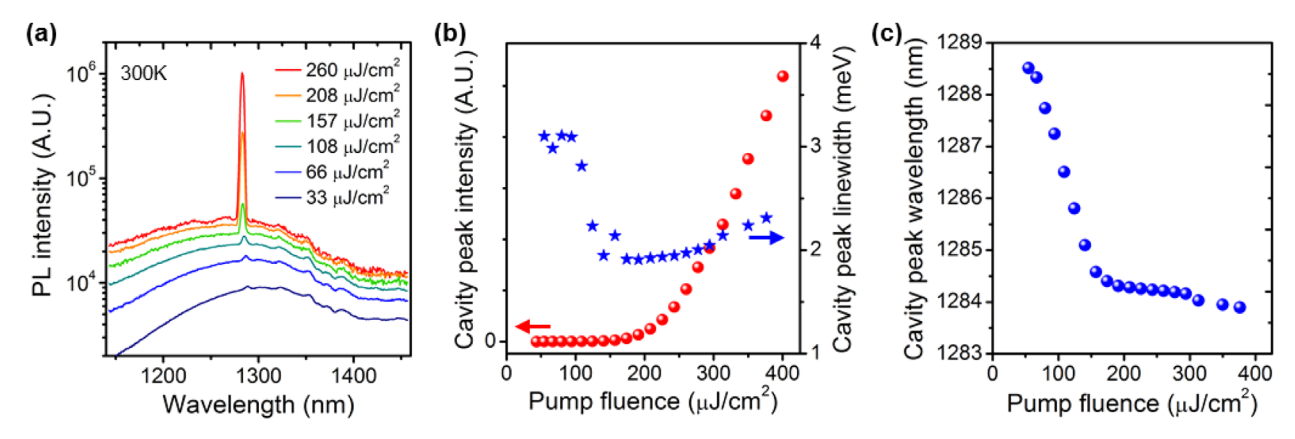


Figure 3. a) PL spectra at various pump fluences plotted in a log scale. b) Light-light curve of the cavity peak intensity plotted together with the cavity linewidth. c) Cavity peak wavelength as a function of the pump fluence.

and starts to grow. The stimulated emission peak quickly dominates spontaneous emission spectra, reaching a side-mode suppression ratio (SMSR) of 14dB at the pump fluence of 260 µJ cm⁻², which is the ratio between the amplitude of the lasing peak and the strongest side peak (spontaneous peak in our case). The lasing wavelength agrees perfectly with the calculated cavity wavelength derived from FDTD simulations (1286 nm), confirming that the lasing mode is fundamental M-point bandedge mode. The pump fluence-dependent emission behavior is further studied by subtracting the spontaneous emission peak from the measured spectra. As shown in the light-light curve in Figure 3b, the cavity peak intensity, which is an integrated intensity of the cavity peak after subtracting the spontaneous emission, shows a clear lasing onset around 200 μ J cm⁻². This is also confirmed from the cavity peak linewidth, where the linewidth is relatively large below the lasing threshold and decreases to its minimum around 180 µJ cm⁻² by increasing the pump power. When the pump power is above the threshold, on the other hand, the cavity peak linewidth starts to increase monotonically with the pump fluence. This is because the fluctuation of the carrier density under pulsed pumping condition is larger at higher pump fluence, and larger fluctuation of the carrier density results in larger fluctuation of the refractive index of active media that affects the resonance wavelength. [35] These results also agree with other reports. [36,37] Another interesting feature is the shift of cavity peak wavelength as a function of the pump fluence. As shown in Figure 3c, the peak wavelength abruptly drops by increasing the pump power when below the lasing threshold (1288.5 nm at $55 \,\mu\text{J cm}^{-2}$ to $1284.4 \,\mathrm{nm}$ at $174 \,\mu\mathrm{J}\,\mathrm{cm}^{-2}$). On the other hand, the peak wavelength decreases much slowly above the threshold, reaching 1283.9 nm at 376 µJ cm⁻². This is also attributed to the change of the refractive index of InGaAs nanowires as a function of the carrier density. At a low pump power, the carrier lifetime is relatively long and so the carrier density in conduction bands proportionally increases with the pump power. Because of the increased carrier density, the refractive index decreases, [35] which shifts the resonant frequency of cavities to shorter wavelength. On the contrary, the carrier lifetime becomes much shorter above the lasing threshold due to stimulated recombination, bringing the lifetime down to the level of picoseconds which is

the similar order as the pump pulse. [16,38] Therefore, the carrier density does not proportionally increase with the pump power anymore due to the fast de-population of carriers, and this leads to much slower decrease of the cavity peak wavelength above threshold. We note that the peak wavelength continues to blueshift even at the highest pump fluence. This indicates that the heating of nanowires is negligible at this power, since elevated temperature of InGaAs will increase the refractive index and this will redshift the cavity peak wavelength. [39–41] In other words, the cavity peak position measured as a function of the pump fluence indicates that the InGaAs nanowires passivated with InP shells have high quantum efficiency, which has led to stable room-temperature operation.

In ultracompact lasers, spontaneous emission factor, β , which represents the portion of spontaneously emitted photons coupled to the lasing mode, is one of the important parameters to investigate the nature of thresholdless lasers and is typically larger than conventional lasers. We have extracted β and Q factor of the fabricated laser by fitting the measured light-light curve with rate equations which take into account optical pumping conditions. [16,23] The rate equations and parameters used for the fitting are detailed in Experimental Section. Figure 4 shows double-logarithmic light-light curve, which is plotted with theoretically derived curves using the rate equation model. The measured data show good agreement with the rate equation model when $\beta = 0.014$ and Q = 1350. The spontaneous emission factor of 0.014 is much larger than that of conventional VCSEL or DFB lasers which typically exhibit β on the order of 10^{-4} or 10^{-5} [42] Such a large β originates from extremely small mode volume of the proposed laser, and large β is beneficial for low-threshold lasing and energy-efficient operation of lasers. The extracted cavity O factor of 1350 is significantly smaller than the theoretically predicted cavity O factor of 23 000, although it is still larger than single nanowire-type lasers. This discrepancy stems from the non-uniformity in the dimension of 2D gratings, and the Q factor could be improved by optimizing silicon dry-etching conditions. The Q factor can also be further enhanced by improving the uniformity of nanowires by optimizing growth conditions, although it should be noted that the non-uniformity of nanowires is not related to edge effects since nanowires in the edge and center of the array exhibit the same average diameter.



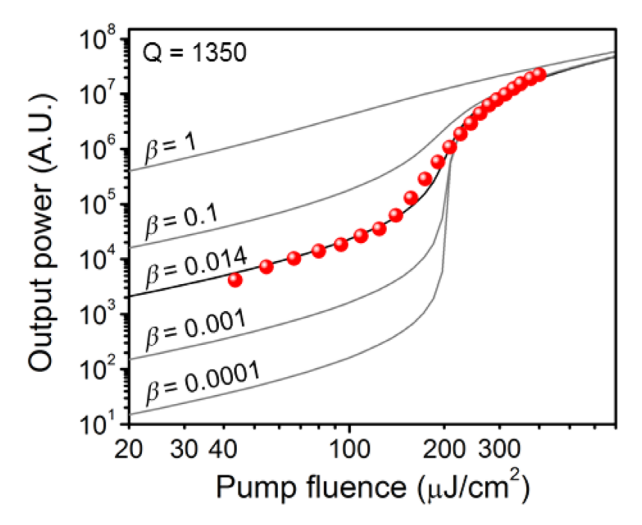


Figure 4. Double-logarithmic light-light curve of measured data (red dots) plotted with theoretical curves derived from rate equation models under various β (gray lines). The measured data agrees well with the rate equation model when $\beta = 0.014$ and Q = 1350.

In conclusion, we have demonstrated InGaAs nanowire array band-edge lasers on silicon-on-insulator platforms with 2D silicon gratings. The fabricated laser operated at 1290 nm at room temperature by optical pumping, and exhibited robust emission without any signature of heating or degradation. The nanowire laser is integrated on 220 nm-thick SOI with pre-defined patterns, suggesting that the proposed laser could be integrated on silicon photonic platforms with various components such as waveguides, grating couplers, and modulators. We therefore believe that the proposed ultracompact lasers on silicon could be potentially employed for many application fields including photonic integrated circuits (PICs), on-chip photonic interconnects, and chemical/bio sensors.

Experimental Section

Nanowire Growth: The nanowire growth is carried out in Emcore D-75 vertical MOCVD reactor at 60 Torr. Native oxide on the sample is etched by buffered oxide etch (BOE) solution for 20 s followed by rinsing with deionized water, and then the sample is directly loaded into the reactor. High-temperature baking at 850 °C for 10 min in the reactor is carried out as an additional oxide etching step, and then the reactor temperature is decreased to 680 °C. GaAs seeds are first grown for 3 min in nanoholes by flowing TEGa of $8.78 \times 10^{-7} \, \text{mol min}^{-1}$ and TBAs of $7.93 \times 10^{-5} \, \text{mol min}^{-1}$, which improves the vertical growth of InGaAs nanowires. [24,43] Then, InGaAs nanowires are grown at $655 \, ^{\circ}\text{C}$ by flowing TEGa of $6.32 \times 10^{-7} \, \text{mol min}^{-1}$, TMIn of $5.16 \times 10^{-7} \, \text{mol min}^{-1}$ and TBAs of $7.93 \times 10^{-5} \, \text{mol min}^{-1}$ for $13 \, \text{min}$. Finally, InP shells are grown at $600 \, ^{\circ}\text{C}$ by flowing TMIn = $4.04 \times 10^{-7} \, \text{mol min}^{-1}$ and TBP = $6.09 \times 10^{-5} \, \text{mol min}^{-1}$ for $35 \, \text{s}$. The reactor is then cooled down under TBP overpressure to prevent the desorption of InP shells.

Optical Characterization: The emission from fabricated lasers is characterized using a microphotoluminescence (μ PL) setup at room temperature. A pulsed supercontinuum laser (SuperK EXTREME EXW-12) with a wavelength of 660 nm, repetition rate of 1.95 MHz and a pulse width of 30 ps is used for optical pumping, and an objective lens is used to

focus the beam onto nanowire arrays from vertical direction, where the beam spot size on the sample is approximately $2\,\mu m$. The emission from nanowires is collected by the same lens and resolved by a spectrometer (Acton SP-2500i) equipped with a commercial InGaAs detector (2D-OMA). A longpass filter is used to prevent the pump light from reaching the detector.

Rate Equation Analysis: Rate equations for the carrier density (N) and the photon density (P) are expressed as

$$\frac{dN}{dt} = \frac{\eta P}{\hbar \omega_p V} - AN - \frac{N}{\tau_{sp}} - CN^3 - \nu_g GS \tag{1} \label{eq:dN}$$

$$\frac{dS}{dt} = \left[\Gamma \nu_g G - \frac{1}{\tau_n} \right] S + \Gamma \beta \frac{N}{\tau_{\nu_D}} \tag{2}$$

where in η is the absorbed portion of the pump light, P is the average power of the pump light, and V is the volume of active media. We have adopted the Shockley-Read-Hall (SRH) coefficient of $A=1.43\times 10^8$ s⁻¹,^[16] the radiative lifetime of $\tau_{sp}=4$ ns,^[16] and the Auger recombination coefficient of $C=2.44\times 10^{-29}$ cm⁶s⁻¹.^[44] The gain, G, is estimated using $G(N)=g_0\ln\frac{(N+N_{tr})}{N+N_s}$, where the gain coefficient $g_0=3050\,\mathrm{cm}^{-1}$, the transparent carrier density $N_{tr}=1.14\times 10^{18}\,\mathrm{cm}^{-3}$, and the third linearity parameter $N_s=9.95\times 10^{17}\,\mathrm{cm}^{-3}$ are adopted from our previous report.^[24] The confinement factor $\Gamma=0.52$ is derived from FDTD simulations, and the group velocity ν_g is assumed to be 4. Last, the photon lifetime, τ_p , and the spontaneous emission factor, β , are used as fitting parameters

Acknowledgements

H. Kim and W.-J. Lee contributed equally to this work. The authors acknowledge the generous financial support of this research by Air Force Office of Scientific Research (FA9550-15-1-0324), National Science Foundation (ECCS-1711967), Institute for Information & communications Technology Promotion (IITP) grant funded by the Korea government (MSIT) (No.20170000740011001, A Generic Technology Study for Quantum Photonic Integrated Circuits) and Sêr Cymru grants in Advanced Engineering and Materials.

Keywords

InGaAs, nanowires, nanolasers, photonic crystals, silicon photonics

Received: September 17, 2018 Revised: November 7, 2018 Published online: November 27, 2018

- [1] C. Gunn, IEEE Micro 2006, 26, 58.
- [2] G. Roelkens, L. Liu, D. Liang, R. Jones, A. Fang, B. Koch, J. Bowers, Laser Photonics Rev 2010, 4, 751.
- [3] Z. Zhou, B. Yin, J. Michel, Light: Sci. Appl. 2015, 4, e358.
- [4] H. Wada, T. Kamijoh, IEEE Phot. Technol. Lett. 1996, 8, 173.
- [5] H. Park, A. W. Fang, S. Kodama, J. E. Bowers, Opt. Expr. 2005, 13, 9460.
- [6] S. Chen, W. Li, J. Wu, Q. Jiang, M. Tang, S. Shutts, S. N. Elliott, A. Sobiesierski, A. J. Seeds, I. Ross, Nat. Photon. 2016, 10, 307.
- [7] T. Mårtensson, C. P. T. Svensson, B. A. Wacaser, M. W. Larsson, W. Seifert, K. Deppert, A. Gustafsson, L. R. Wallenberg, L. Samuelson, *Nano Lett.* 2004, 4, 1987.



www.advancedsciencenews.com

- [8] G. Xing, N. Mathews, S. S. Lim, N. Yantara, X. Liu, D. Sabba, M. Grätzel, S. Mhaisalkar, T. C. Sum, Nat. Mat. 2014, 13, 476.
- [9] P. Cegielski, A. L. Giesecke, S. Neutzner, C. Porschatis, M. Gandini, D. Schall, C. Perini, J. Bolten, S. Suckow, S. Kataria, Nano Lett. 2018,
- [10] H. Zhu, Y. Fu, F. Meng, X. Wu, Z. Gong, Q. Ding, M. V. Gustafsson, M. T. Trinh, S. Jin, X. Zhu, Nat. Mat. 2015, 14, 636.
- [11] O. Salehzadeh, M. Djavid, N. H. Tran, I. Shih, Z. Mi, Nano Lett. 2015,
- [12] P. Caroff, K. A. Dick, J. Johansson, M. E. Messing, K. Deppert, L. Samuelson, Nat. Nanotechnol. 2009, 4, 50.
- [13] E. Ertekin, P. A. Greaney, D. Chrzan, T. D. Sands, J. Appl. Phys. 2005,
- [14] J. C. Johnson, H.-J. Choi, K. P. Knutsen, R. D. Schaller, P. Yang, R. J. Saykally, Nat. Mat. 2002, 1, 106.
- [15] X. Duan, Y. Huang, R. Agarwal, C. M. Lieber, Nature 2003, 421, 241.
- [16] R. Chen, T.-T. D. Tran, K. W. Ng, W. S. Ko, L. C. Chuang, F. G. Sedgwick, C. Chang-Hasnain, Nat. Phot. 2011, 5, 170.
- [17] B. Mayer, L. Janker, B. Loitsch, J. Treu, T. Kostenbader, S. Lichtmannecker, T. Reichert, S. Morkötter, M. Kaniber, G. Abstreiter, Nano Lett. 2015, 16, 152.
- [18] F. Lu, I. Bhattacharya, H. Sun, T.-T. D. Tran, K. W. Ng, G. N. Malheiros-Silveira, C. Chang-Hasnain, Optica 2017, 4,
- [19] T. Stettner, T. Kostenbader, D. Ruhstorfer, J. Bissinger, H. Riedl, M. Kaniber, G. Koblmüller, J. J. Finley, ACS Phot. 2017, 4, 2537.
- [20] W.-J. Lee, H. Kim, A. C. Farrell, P. Senanayake, D. L. Huffaker, Appl. Phys. Lett. 2016, 108, 081108.
- [21] D.-X. Xu, J. H. Schmid, G. T. Reed, G. Z. Mashanovich, D. J. Thomson, M. Nedeljkovic, X. Chen, D. Van Thourhout, S. Keyvaninia, S. K. Selvaraja, IEEE J. Selected Topics Quantum Electr. 2014, 20, 189.
- [22] W.-J. Lee, H. Kim, J.-B. You, D. L. Huffaker, Sci. Rep. 2017, 7, 9543.
- [23] H. Kim, W.-J. Lee, A. C. Farrell, J. S. Morales, P. Senanayake, S. V. Prikhodko, T. J. Ochalski, D. L. Huffaker, Nano Lett. 2017, 17, 3465.
- [24] H. Kim, W.-J. Lee, A. C. Farrell, A. Balgarkashi, D. L. Huffaker, Nano Lett. 2017, 17, 5244.

- [25] K. Komolibus, A. C. Scofield, K. Gradkowski, T. J. Ochalski, H. Kim, D. L. Huffaker, G. Huyet, Appl. Phys. Lett. 2016, 108, 061104.
- [26] H. Dinges, H. Burkhard, R. Lösch, H. Nickel, W. Schlapp, Appl. Surf. Sci. 1992, 54, 477.
- [27] T. Xu, S. Yang, S. V. Nair, H. Ruda, Phys. Rev. B 2005, 72, 045126.
- [28] K. Sakai, E. Miyai, T. Sakaguchi, D. Ohnishi, T. Okano, S. Noda, IEEE J. Sel. Areas Commun. 2005, 23, 1335.
- [29] Y. Akahane, T. Asano, B.-S. Song, S. Noda, Nature 2003, 425, 944.
- [30] S. Kim, S. Ahn, J. Lee, H. Jeon, P. Regreny, C. Seassal, E. Augendre, L. Di Cioccio, Opt. Expr. 2011, 19, 2105.
- [31] H. Kim, A. C. Farrell, P. Senanayake, W.-J. Lee, D. L. Huffaker, Nano Lett. 2016, 16, 1833.
- [32] L. Xu, Q. Huang, IEEE Trans. Nanotechnol. 2014, 13, 1093.
- [33] M. T. Borgström, G. Immink, B. Ketelaars, R. Algra, E. P. Bakkers, Nat. Nanotechnol. 2007, 2, 541.
- [34] J. Shapiro, A. Lin, P. Wong, A. Scofield, C. Tu, P. Senanayake, G. Mariani, B. Liang, D. Huffaker, Appl. Phys. Lett. 2010, 97, 243102.
- [35] B. R. Bennett, R. A. Soref, J. A. Del Alamo, IEEE J. Quantum Electr. **1990**. 26. 113.
- [36] Z. Wang, B. Tian, M. Pantouvaki, W. Guo, P. Absil, J. Van Campenhout, C. Merckling, D. Van Thourhout, Nat. Photonics 2015, 9, 837.
- [37] J. Tatebayashi, S. Kako, J. Ho, Y. Ota, S. Iwamoto, Y. Arakawa, Nature Photonics 2015, 9, 501.
- [38] H. Altug, D. Englund, J. Vučković, Nat. Phys. 2006, 2, 484.
- [39] J. McCaulley, V. Donnelly, M. Vernon, I. Taha, Phys. Rev. B 1994, 49, 7408.
- [40] Y. Gong, B. Ellis, G. Shambat, T. Sarmiento, J. S. Harris, J. Vučković, Opt. Expr. 2010, 18, 8781.
- [41] J. Pan, Y. Huo, K. Yamanaka, S. Sandhu, L. Scaccabarozzi, R. Timp, M. L. Povinelli, S. Fan, M. Fejer, J. S. Harris, Appl. Phys. Lett. 2008, 92,
- [42] L. A. Coldren, S. W. Corzine, M. L. Mashanovitch, Diode lasers and photonic integrated circuits. John Wiley & Sons, New York, USA 2012.
- [43] H. Kim, D. Ren, A. C. Farrell, D. L. Huffaker, Nanotechnology 2018, 29, 085601.
- [44] T. Gfroerer, L. Priestley, M. Fairley, M. Wanlass, J. Appl. Phys. 2003, 94, 1738.